Characteristics of Oxygen Electrode Supported Reversible Solid Oxide Cells

Shan-Lin Zhang[a,b1], Hongqian Wang[b,1], Tianrang Yang[c], Matthew Y. Lu[b], Scott A. Barnett[b,*]

[a] School of Chemical Engineering and Technology, Sun Yat-sen University, Zhuhai campus, Zhuhai, Guangdong, 519082, P. R. China

[b] Department of Materials Science and Engineering, Northwestern University, Evanston, Illinois 60208, USA

c Key Laboratory of Power Station Energy Transfer Conversion and System of MOE, School of Energy Power and Mechanical Engineering, North China Electric Power University, 2 Beinong Road, Changping District, Beijng 102206, P. R. China

[1] These authors contributed equally to this work.

Abstract

Oxygen-electrode-supported solid oxide cells (OESCs) have potential advantages over fuel-electrode-supported cells, including reduced fuel-electrode concentration polarization, better oxygen electrode current collection, and flexibility in the fuel electrode choice. However, there are serious drawbacks including the difficulty of co-firing the oxygen electrode and electrolyte, and oxygen electrode concentration polarization. This paper explores the characteristics of OESCs with $La_{0.8}Sr_{0.2}MnO_3$-$Zr_{0.92}Y_{0.16}O_2$ (LSM-YSZ) electrode-support enhanced by $SrTi_{0.3}Fe_{0.6}Co_{0.1}O_{3-\delta}$ (STFC) infiltration, thin YSZ electrolyte, and $SrTi_{0.3}Fe_{0.7}O_{3-\delta}$ (STF) fuel electrodes. The STFC infiltration increases fuel cell maximum power density by > 1.5 times and electrolysis current density (at 1.3 V) by >

2 times. Cell performance in pure oxygen is compared to that in air, exploring a possible reversible solid oxide cell system configuration where oxygen produced during electrolysis is stored and subsequently used during fuel cell operation. The fuel cell maximum power density is increased from 0.88 W cm^{-2} in air to 1.37 W cm^{-2} in oxygen, with limiting current increased from 1.7 to >5.6 A cm^{-2}; the electrolysis performance is essentially unchanged, probably because the electrode air becomes enriched with oxygen during electrolysis.

Keywords: Solid Oxide Cells; Oxygen Electrode Support; Electrolysis; Reversible; Characteristics

1. Introduction

Solid oxide cells (SOCs) have received increasing attention for electrolytic fuel production from renewable electricity and as reversible electrical energy storage devices.[1-8] Much of the SOC research and development has focused on fuel-electrode-supported cells that provide outstanding performance in fuel cell applications. For electrolysis and reversible energy-storage applications, oxygen-electrode-supported cell designs have potential advantages. That is, the fuel electrode can be significantly thinner than in a fuel-electrode-supported cell, alleviating gas diffusion concentration polarization that may limit steam utilization during electrolysis and fuel utilization in fuel cell operation.[9-11] Furthermore, since the fuel electrode is fired last during cell processing, a wide range of fuel-electrode materials choices is available; this has already been shown to provide improved performance in OESCs.[12] These advantages are also present for electrolyte-supported cells, but they have the disadvantage of relatively high electrolyte resistance. The OESC disadvantage of having a thick oxygen electrode support may be mitigated in

some cases. In SOC electrolysis, the oxygen produced during operation tends to displace air within the oxygen electrode at the high current densities, which should mitigate the significant gas diffusion limitations encountered with thick oxygen electrode supports when working with air.[13] In a reversible SOC application, the oxygen produced during electrolysis could potentially be stored and then used instead of air during fuel cell operation;[2] again helping to mitigate mass transport limitations.

Processing issues pose a significant barrier to the realization of high-performance oxygen-electrode-supported cells. First, most oxygen-electrode materials have much lower melting temperature than electrolyte materials, making it difficult to find a processing temperature where the electrolyte is densified while retaining sufficient electrode porosity, surface area, and three-phase boundary (TPB) density. This is exacerbated by the fact that common oxygen electrodes such as LSM-YSZ require higher TPB density than Ni-YSZ fuel electrodes in order to achieve low polarization resistance.[14] Second, the high co-firing temperature may cause electrode/electrolyte reactions and/or interdiffusion. Thus, it is critical to reduce the electrolyte sintering temperature to allow co-firing of the electrolyte and oxygen electrode. For example, sintering aids have been used to enable single-step firing of entire fuel-electrode-supported SOCs, including the NiO-$Y_{0.16}Zr_{0.92}O_{2-\delta}$ (YSZ) electrode, YSZ electrolyte, and $(La_{0.8}Sr_{0.2})_{0.98}MnO_{3-\delta}$ (LSM)-YSZ or $(La_{0.85}Ca_{0.15})_{0.97}MnO_{3-\delta}$-YSZ electrodes.[15-17] The resulting cells had electrodes with good porosity, dense electrolytes, were free of significant elemental interdiffusion, and yielded good cell performance. However, it was shown that the LSM-YSZ electrodes had a relatively low TPB density and hence higher polarization resistance compared to traditional two-step

fired cells, due to the higher firing temperature and free shrinkage during co-firing. It is expected that similar processing conditions can be used for fabrication of oxygen-electrode-supported cells. Alternatively, various infiltration strategies,[18, 19] such as $SrTi_{0.3}Fe_{0.6}Co_{0.1}O_{3-\delta}$ (STFC) have been employed to produce improved oxygen electrodes – this approach is desirable because it provides a simple way to enhance standard LSM-YSZ-electrode SOCs.[20]

In this work, we characterize oxygen-electrode-supported SOCs consisting of LSM-YSZ oxygen-electrode and support, YSZ electrolyte, and $SrTi_{0.3}Fe_{0.7}O_{3-\delta}$ (STF) fuel electrode, made using a reduced-temperature firing process. Note that STF was previously shown to provide similar performance as Ni-YSZ as the fuel electrode.[12] The electrochemical characteristics are studied, using current-voltage measurements and impedance spectroscopy, with both air and pure oxygen at the oxygen electrode. Enhancement of the LSM-YSZ electrode by STFC infiltration is found to be critical for obtaining high cell power density and electrolysis current density.

2. Experimental

2.1 Materials Synthesis and Cell Fabrication Process

The solid-state reaction method was used to synthesize the STF fuel electrode powder. The detailed synthesis process can be found elsewhere [21, 22]. LSM-YSZ supported half cells were prepared by tape casting with 38.5 wt.% LSM (Praxair, d_{50} = 1.1 μm) + 41.5 wt.% YSZ (Tosoh, surface area = 6.2 $m^2 g^{-1}$) + 8 wt.% Tapioca starch (pore former) + 12 wt.% graphite (pore former, Timcal, Switzerland, average size: 2.2 μm) as the support layer, 38.5 wt.% LSM + 38.5 wt.% YSZ + 23 wt.% graphite (pore former) as the oxygen electrode

functional layer, and YSZ as the electrolyte. In order to reduce the firing temperature, 3 mol% Fe_2O_3 sintering aid was added in the electrolyte formulation with YSZ (Tosoh). Then the cells were co-fired at 1225 °C for 2 h. Next, in order to prevent reactions between the YSZ electrolyte and STF anodes, a GDC interlayer was screen printed on the YSZ electrolyte and fired at 1175 °C for 2 h. Finally, the STF fuel electrode was screen printed onto the GDC interlayer and fired at 1050 °C for 4 h. The STF fuel electrode had a circular area of 0.5 cm^2, centered on the button cell with area of ~ 2 cm^2 (16 mm in diameter). For some cells, STFC was infiltrated into the LSM-YSZ support oxygen electrode to improve its performance.[12, 20] The STFC precursor solution concentration was 0.25 mol L^{-1}. Cells were heated to 450 °C for 0.5 h after each infiltration. Each electrode was infiltrated 4 times, resulting in a 4.0 mg STFC deposition, corresponding to ~ 12 vol% STFC in the electrode. After 4 infiltration steps, the cells were fired at 800 °C for 1 h to form STFC in air at the beginning of cell testing. The full detailed infiltration process can be found elsewhere.[20]

2.2 Cell Characterization

Before the cell testing, a gold grid (Heraeus Inc., Pennsylvania) was screen printed onto the STF electrode for current collection. The cells were sealed onto alumina tubes with silver paste (DAD-87, Shanghai Research Institute of Synthetic Resins). Current–voltage characteristic (with 20 mV increments) and electrochemical impedance spectroscopy (EIS) measurements were carried out in the temperature range from 700–800 °C. Either 150 sccm air or pure oxygen were supplied to the LSM-YSZ electrode support. During electrolysis testing, the fuel electrode was supplied with 100 sccm H_2

flowed through a heated H_2O-containing bubbler maintained at 81.3 °C, entraining 50% water in the H_2 flow. During fuel cell testing, 100 sccm H_2 was flowed through the ambient temperature bubbler, suppying 97% H_2 + 3% H_2O to the fuel electrode. The EIS measurements were conducted using an IM6 Electrochemical Workstation (ZAHNER, Germany) at open circuit voltage with a 20 mV AC signal in the frequency range of from 0.1 Hz to 100 kHz. After the performance testing, cell microstructures were examined via scanning electron microscopy (SEM) using a Hitachi SU8030 microscope.

3. Results

3.1 Microstructure analysis

Fig. 1 (a) shows a representative polished cross-sectional SEM image of a typical cell after electrochemical testing. The LSM-YSZ support and oxygen electrode functional layer have thicknesses of 700 and 20 μm, respectively. From a stereological analysis of the higher magnification images, porosities are 38.3% for the support layer and 37.1% for the functional layer, similar to the values for LSM-YSZ electrodes prepared by similar procedures as reported in a previous study (36.5%).[15] The LSM-YSZ functional layer has a Triple-Phase Boundary (TPB) density of ~ 1.72 μm^{-2}, close to the values for the similar co-fired LSM-YSZ in the previous study (1.64 μm^{-2}). [15] Two types of pores are visible in the support layer. The larger pores are formed from starch added to the support slurry and have a size of 5–10 μm, while the finer pores are formed from added graphite, with a size < 1 μm. We believe that this dual pore structure should help to minimize gas diffusion concentration polarization. No starch was used in the oxygen electrode functional layer formulation, and hence only finer pores formed from graphite are present – this is believed

to maximize the TPB density and, in the case of the STFC-infiltrated electrodes, to maximize the STFC surface area. Fig.1 (b) shows a higher magnification image of the cell active region. The YSZ electrolyte has a thickness of ~ 6–8 μm and shows a few small closed pores with low enough volume fraction that they are presumably isolated. The LSM-YSZ functional layer and GDC interlayer are bonded well with the YSZ electrolyte. The GDC interlayer has a thickness of 2–3 μm and has a porous structure typical of GDC barriers fired after the high-temperature electrolyte sintering.[23-25] The screen-printed STF fuel electrode has a thickness of 8–10 μm and bonded well with the GDC interlayer. The STF layer has a porous structure with a fine particle size – prior characterization of these electrodes indicates an STF surface area of 4.6 μm^{-1} and a porosity of 38%.[12]

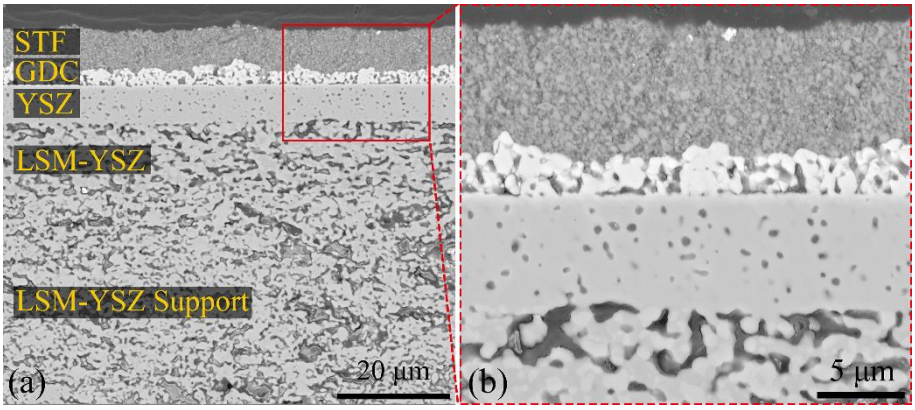

Fig. 1 Polished cross sectional SEM image of the cell (a) and a higher-magnification image of the cell's active region (b).

Fig. 2 shows cross-sectional SEM images of the un-infiltrated (a) and STFC-infiltrated (b) LSM-YSZ functional layer. The un-infiltrated electrode (Fig. 2 (a)) has particles that are bonded well together and have smooth surfaces, similar to previously-reported powder-

processed LSM-YSZ electrodes. [15] As shown in Fig. 2 (b), the STFC-infiltrated LSM-YSZ functional layer has a structure very similar to that of the un-infiltrated LSM-YSZ. This suggests that the infiltrated STFC forms a continuous coating on the LSM-YSZ surface rather than nanoparticles, as observed previously.[20]

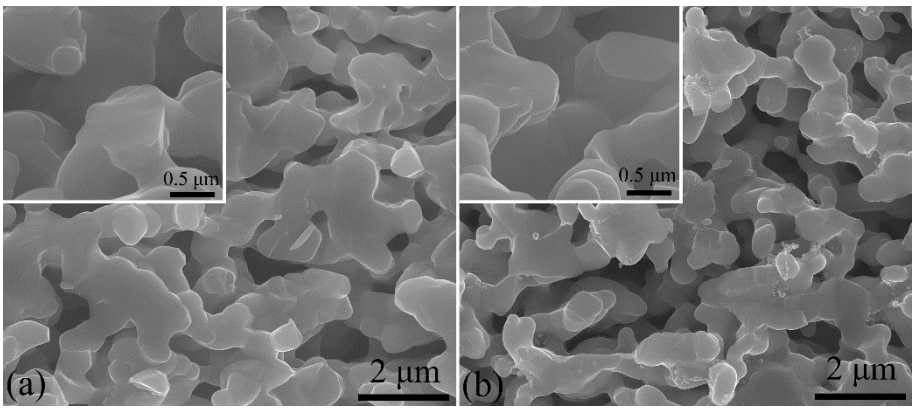

Fig. 2 Fracture cross-sectional SEM images of the un-infiltrated (a) and STFC-infiltrated (b) LSM-YSZ functional layer.

3.2 Effect of STFC Infiltration

The electrochemical characteristics of OESCs made with and without STFC infiltration are compared in Fig. 3. The open-circuit voltage values at 800 °C are ~1.06-1.07 V, similar to the values reported previously under the same conditions in this cell test setup.[26] This suggests that the electrolyte in the OESCs fired at 1225 °C is sufficiently dense to avoid gas significant leakage, consistent with the SEM images in Fig. 1. The maximum fuel cell power density is higher for the STFC-infiltrated cell, *e.g.* 0.88 W cm^{-2} at 800 °C compared to 0.57 W cm^{-2} without STFC (Fig. 3a). The electrolysis current density is also substantially higher, *e.g.*, 1.32 A cm^{-2} at 800 °C at a typical electrolysis voltage of 1.3 V, compared to 0.65 A cm^{-2} without STFC (Fig. 3 (c)). The relatively low current and power densities of the non-infiltrated cell are similar to those

reported previously for LSM-YSZ co-fired with YSZ, and were explained by the relatively high polarization resistance of the co-fired LSM-YSZ oxygen electrode, a result of the non-ideal electrode microstructure and also the possible presence of a zirconate phase.[15] The substantially improved oxygen electrode performance after STFC infiltration agrees with a prior report, which also demonstrated that the infiltrated electrode provides good stability over ~ 800 h life tests.[20]

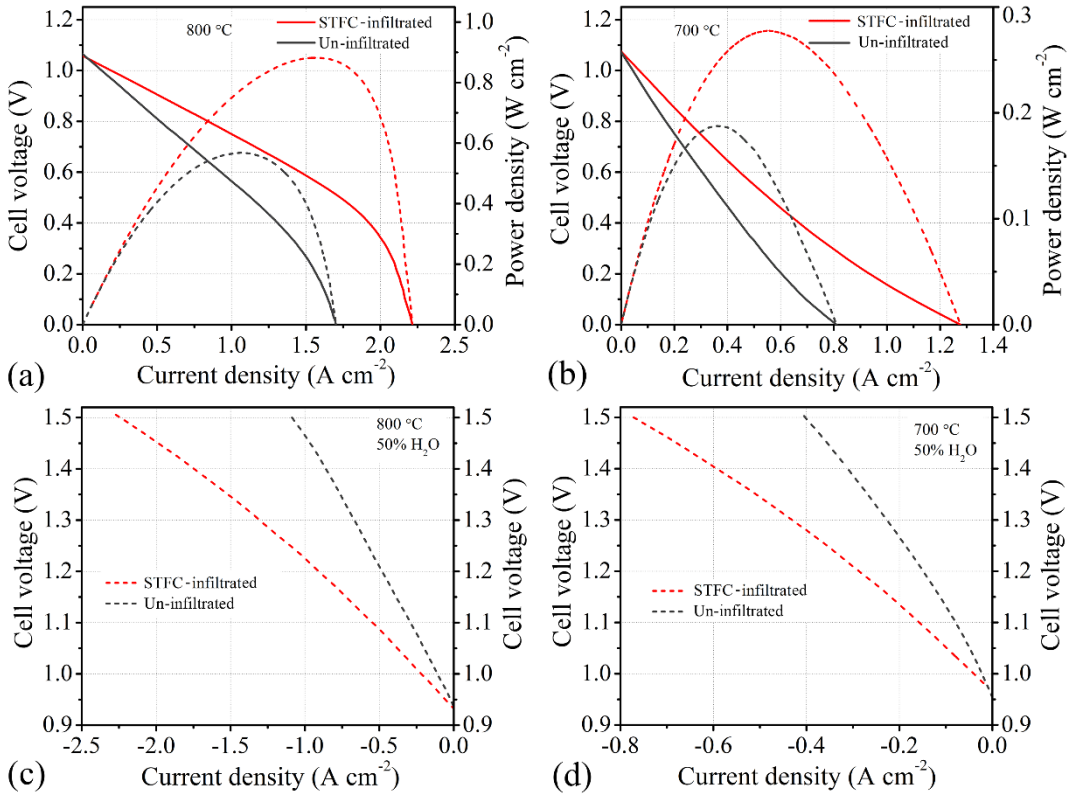

Fig. 3. Fuel cell voltage and power density versus current density for un-infiltrated and STFC-infiltrated cells measured in air and 97% H_2 - 3% H_2O at 800 °C (a) and 700 °C (b). Electrolysis voltage versus current density for un-infiltrated and STFC-infiltrated cells measured in air and 50% H_2 - 50% H_2O at 800 °C (c) and 700 °C (d).

Fig. 4 compares the EIS spectra for cells with un-infiltrated and STFC-infiltrated oxygen electrodes measured at 800 °C in air and 97% H_2 - 3% H_2O. The STFC infiltration

yields a decrease in the total polarization resistance, consistent with the improved fuel cell and electrolysis performance noted above. The EIS data were modeled using an equivalent circuit consisting of an inductor (L), ohmic resistor (R_{ohm}), and three resistor-constant phase element (R-QPE) units in series. [20] The three main responses are shown separately as dashed lines in Fig. 4, along with the cumulative fits shown as solid lines. STFC infiltration significantly reduces the response peaking at ~20 Hz, from ~0.19 Ω cm^2 for the un-infiltrated LSM-YSZ to ~0.05 Ω cm^2 and shifts it to ~ 100 Hz. The small peak centered at ~ 1000 Hz decreases slightly due to STFC infiltration. These results strongly suggest that these responses are associated with the oxygen electrode (R_{oxy}), and are consistent with prior reports on the effect of STFC infiltration into LSM-YSZ.[20] The improvements due to STFC infiltration can be attributed to previously-demonstrated activity of STFC surfaces for the oxygen reduction reaction, especially compared to LSM-YSZ where reactions are limited to three-phase boundaries.[21] The response peaking at ~ 0.5 Hz can be associated with the STF fuel electrode electrochemical process based on prior symmetric cell studies.[12] It seems surprising that it increases slightly due to oxygen-electrode infiltration; one possible explanation is that this response is overlapped with an oxygen electrode gas diffusion response that is increased by STFC infiltration due to the associated 12-15% decrease the pore volume.[20]

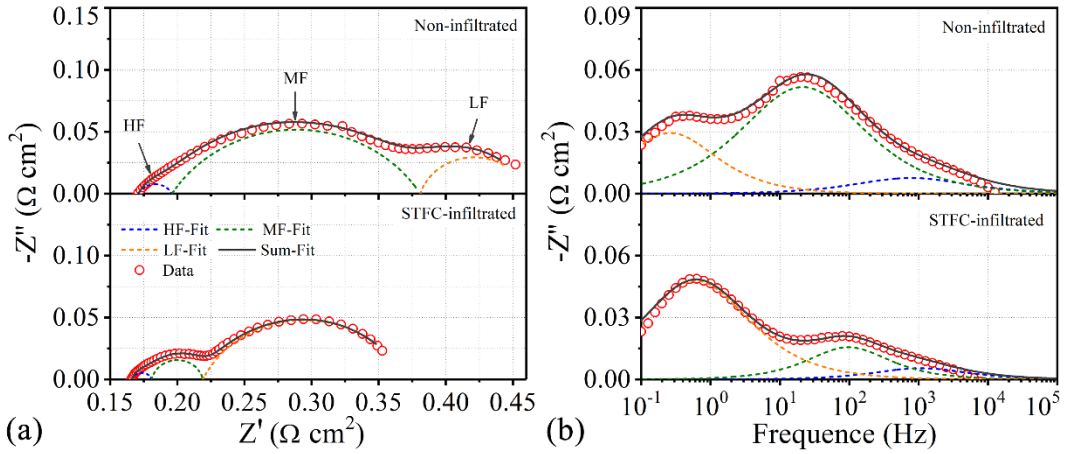

Fig. 4 Nyquist (a) and Bode plots (b) of EIS data measured at 800 °C in 97% H_2 - 3% H_2O and air for cells with un-infiltrated and STFC-infiltrated LSM-YSZ electrodes.

3.3 Effect of Oxidant

Fig. 5 (a) compares the fuel cell characteristics in air and pure oxygen at 800 °C. With air as the oxidant, there is a limiting current density of ~ 2.2 A cm^{-2}, similar to the value in Fig. 3 (a) and in prior reports of OESCs[27, 28]. The limiting current j_L can be calculated as:

$$j_L = zFD_{O_2-N_2}\frac{\varepsilon C_{O_2}}{\tau\delta} \quad (1)$$

where z = 4 (charge transferred per O_2 molecule), F is Faraday's constant, ε is the electrode-support porosity (0.38), τ is the electrode pore tortuosity (~ 1.5), C_{O_2} is the O_2 concentration (2.4×10^{-6} mol/cm^3) at the air flow boundary of the electrode, and δ is the electrode thickness (0.07 cm). The binary O_2-N_2 gas diffusivity $D_{O_2-N_2}$ accounting for bulk and Knudsen diffusion in an electrode with average pore size of ~ 0.5 μm at 800 °C is 0.82 $cm^2\ s^{-1}$.[29] The j_L value obtained using eqn. 1, 2.75 A cm^{-2}, is in reasonable agreement with the measured value, substantiating the idea that the limiting current is due to gas diffusion in the oxygen electrode. Changing the oxidant from air to pure oxygen results in a significant increase in fuel cell maximum power density from 0.88 to 1.37 W cm^{-2}. The

improved performance arises due to three factors: increased open-circuit potential, decreased oxygen electrode polarization resistance (see below), and decreased gas concentration polarization. For pure oxygen, there is no evidence of any limiting current up to at least 5.6 A cm^{-2}, which is reasonable given that C_{O_2} increases by a factor of ~5 in eq. 1. The fuel cell performance at 700 °C (Fig. 5 (b)) is also improved significantly after changing the oxidant from air to pure oxygen, but the current densities are too small to observe a limiting current.

Figure 5 (c) compares the performance of cells tested in air and oxygen, in both fuel cell and electrolysis modes, with 50% H_2 + 50% H_2O at the fuel electrode. Pure oxygen yields a performance improvement in fuel cell mode that is similar to Fig. 5 (a), although the limiting current is slightly lower probably due to cell to cell variations. However, there is little difference between oxygen and air in electrolysis mode. Fig. 5 (d) compares the electrolysis data taken at 800, 750, and 700 ºC. There is no evidence of a limiting current during electrolysis, as expected because the cell is supplying oxygen and hence the electrode cannot become oxygen starved. The strong dependence on temperature and the negative V-j curvature indicate that the current is limited by an activated oxygen evolution reaction. The higher OCV in oxygen versus air means that the electrolysis voltage is generally lower in air; the exception is cell voltages ≥ 1.3 V at 750 and 800 °C because of the slightly lower cell resistance at these temperatures (this may result from different LSM and STFC properties in oxygen versus air).

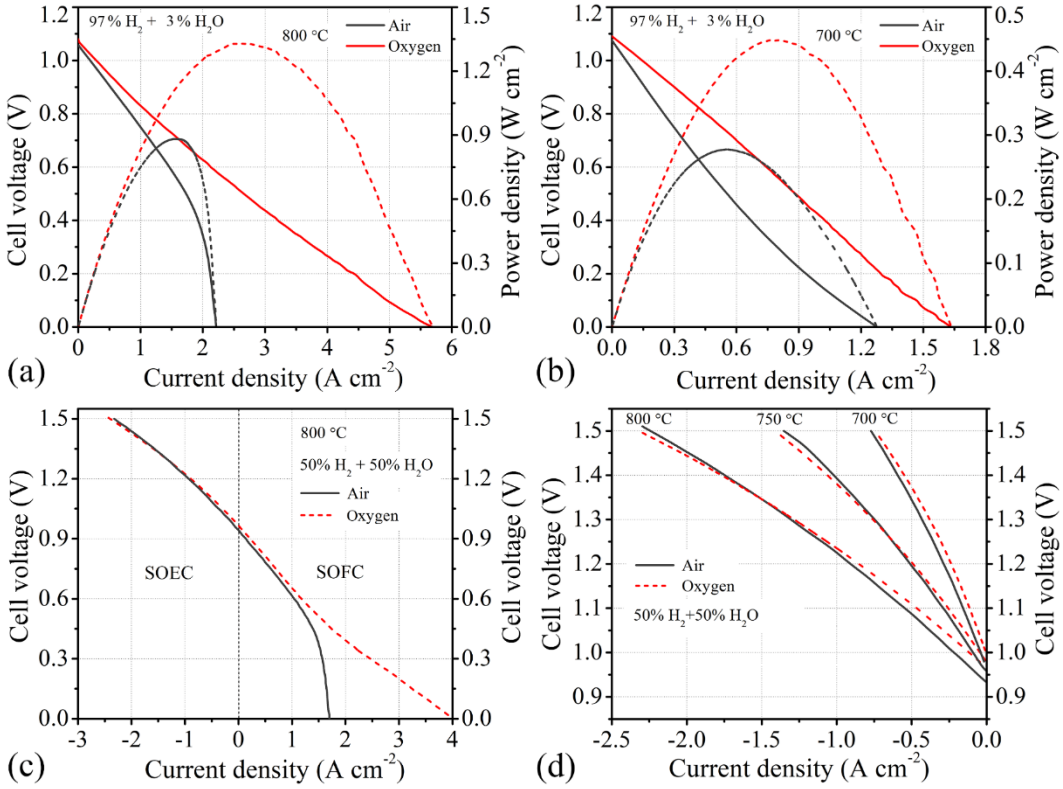

Fig. 5. Voltage and power density versus current density for STFC-infiltrated cells comparing air and oxygen operation: in fuel cell mode with 97% H_2 - 3% H_2O at 800 °C (a) and 700 °C (b); in electrolysis and fuel cell modes with 50% H_2 - 50% H_2O at 800 °C (c); in electrolysis mode with 50% H_2 - 50% H_2O at 700, 750, and 800 °C.

Figure 6 compares the EIS spectra obtained from STFC-infiltrated cells measured in air or oxygen, at 800 °C in 97% H_2 - 3% H_2O. Switching from air to oxygen decreases the oxygen-electrode responses centered at ~ 50 and ~ 1000 Hz. This is consistent with the decrease in cell resistance (lower slope of the j-V curves at low current) in Fig. 5. The response centered at ~0.5 Hz and correlated with the fuel electrode (see Fig. 4 discussion above) shows little effect of switching from air to pure oxygen, as expected. Finaly, the high frequency intercept, probably associated with the cell ohmic resistance, decreased from ~ 0.16 Ω cm^2 to ~ 0.11 Ω cm^2 when pure oxygen was applied. This may indicate a substantial

contribution of oxygen-electrode current collection to the ohmic resistance; the decreased resistance may result from the increased conductivity of LSM in oxygen (~ 200 S sm^{-1}) compared to air (~ 150 S cm^{-1}).[30]

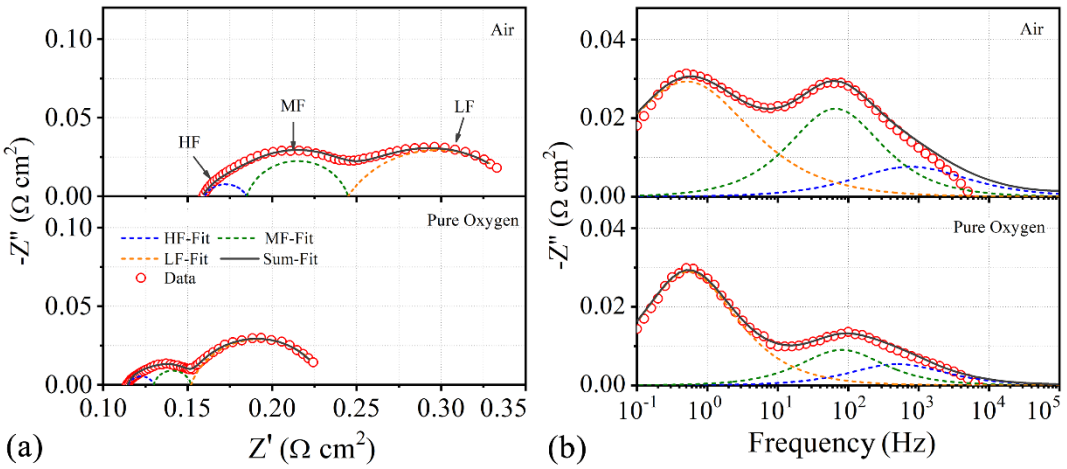

Fig. 6 Nyquist (a) and Bode plots (b) of EIS data from STFC-infiltrated cells measured at 800 °C in 97% H_2 - 3% H_2O, with air or oxygen at the oxygen-electrode.

4. Discussion

The present results show very good oxygen-electrode-supported cell electrolysis performance, with no measurable concentration polarization. The electrolysis current density in the present cells – 1.4 A cm^{-2} at 800 °C and 1.3 V – is less than can be achieved in many fuel-electrode-supported cells; for example, button cells can yield a current density as high as 4 A cm^{-2}.[31] However, fuel-electrode-supported cells may exhibit significant concentration polarization at high steam utilization, which is not expected in the present cells with their relatively thin fuel electrodes. For instance, the current density of Ni-YSZ supported cells at 1.3 V and 800 °C decreased from 2.5 A cm^{-2} for 50% H_2O to 1.5 A cm^{-2} for 20% H_2O, primarily due to concentration polarization.[26] Furthermore, steam depletion

associated with concentration polarization in thick fuel-electrode supports can lead to highly reducing conditions and hence degradation;[32, 33] this is not expected in OESCs due to the relatively thin fuel electrodes. Electrolyte-supported electrolysis cells share the advantage of a relatively thin fuel electrode, but they have a larger electrolyte resistance that typically requires a higher operating temperature of 850 °C to achieve a comparable current density.[34]

In using reversible SOCs for energy storage, the pure oxygen produced during electrolysis could be stored and then used in subsequent fuel cell operation. An initial assessment of the utility of this system design can be made by using the present OESC data. The ideal round-trip voltage efficiency, given by V_{FC}/V_{EL}, can be compared for the stored oxygen case compared to conventional air operation. The results from cell operation at 800 °C (Fig. 5 (c)) are used and a current density of 1 A cm^{-2} in both directions is assumed. Note that the electrolysis voltage is slightly increased by using oxygen (1.24 V) compared to air (1.22 V). However, the fuel cell voltage is higher in oxygen (0.86 V) compared to air (0.75 V). This yields a round-trip cell voltage efficiency improvement from 61% in air to 69% in oxygen. Thus, although the use of pure oxygen minimizes one of the key disadvantages of OESCs – concentration polarization in the thick electrode support in fuel cell mode – the effect at reasonable current densities may not be sufficient to justify storing electrolytically-produced oxygen. Note that this calculus may be different for cells with lower support porosity or lower ASR, where concentration polarization in air could be more dominant.

5. Summary and conclusions

Oxygen electrode supported cells (OESCs) with STFC-infiltrated LSM-YSZ electrode supports and STF fuel electrodes were investigated in this study. Overall cell resistance had significant contributions from the LSM-YSZ-STFC and STF electrodes along with ohmic resistance. STFC infiltration into the LSM-YSZ electrode decreased cell resistance, increasing fuel cell maximum power density by > 50% and electrolysis current density by > 100%. This result, combined with the very good stability previously reported,[20] shows that STFC-infiltrated LSM-YSZ is a promising electrode for OESCs. Further improvement of the cells may be possible by improving the infiltrated oxygen electrode, and also by decreasing the fuel electrode polarization resistance, as shown recently for STF-based exsolution fuel electrodes.[12]

Cells operated in air exhibited a limiting current density of ~ 2 A cm^{-2} in fuel cell mode, whereas there was no limiting current observed in electrolysis mode. Changing the oxidant from air to pure oxygen increases the fuel cell maximum power density at 800 ºC from 0.88 to 1.37 W cm^{-2} and eliminates the limiting current up to the highest current measured, 5.6 A cm^{-2}. The limiting current values agree reasonably well with values predicted for oxygen electrode gas diffusion. Switching from air to oxygen doesn't improve electrolysis performance, due in part to the increased open-circuit potential. Evaluation of the results indicates that reversible SOC operation using stored oxygen in fuel cell mode should yield an improved round-trip voltage efficiency compared to air operation. Furthermore, the concentration polarization in oxygen is reduced enough that cells with lower LSM-YSZ support porosity, providing improved mechanical robustness, should work very well. Further analysis at the stack and system level will be required to determine if these

advantages justify the the additional system complication of storing oxygen. Overall, the present results suggest that oxygen-electrode-supported cells have good potential for electrolysis and reversible storage applications.

Acknowledgements

The authors gratefully acknowledge financial support by the Department of Energy (DE-EE0008437), which supported the electrochemical performance analysis, and Department of Energy grant # DE-SC0016965, which supported much of the cell development. Initial development of the oxygen-electrode-supported cells was done under support from the National Science Foundation (DMR-1912530). Shan-Lin Zhang gratefully acknowledges the scholarship from the State Scholarship Fund of China Scholarship Council (201606285002). This work made use of the EPIC facility of Northwestern University's NUANCE Center, which has received support from the Soft and Hybrid Nanotechnology Experimental (SHyNE) Resource (NSF ECCS-1542205); the MRSEC program (NSF DMR-1121262) at the Materials Research Center; the International Institute for Nanotechnology (IIN); the Keck Foundation; and the State of Illinois, through the IIN. This work made use of the MatCI Facility which receives support from the MRSEC Program (NSF DMR-1720139) of the Materials Research Center at Northwestern University.

Reference

1. M. A. Laguna-Bercero, J. Power Sources, 203 (2012), 4-16.

2. D. M. Bierschenk, J. R. Wilson, S. A. Barnett, Energ Environ. Sci., 4 (2011), 944-951.

3. C. Graves, S. D. Ebbesen, M. Mogensen, Solid State Ionics, 192 (2011), 398-403.

4. Z. Zhan, W. Kobsiriphat, J. R. Wilson, M. Pillai, I. Kim, S. A. Barnett, Energy Fuel, 23 (2009), 3089-3096.

5. M. Mogensen, S. H. Jensen, A. Hauch, I. Chorkendorff, T. Jacobsen, Ceram. Eng. Sci. Proc., 28 (2008), 91-101.

6. A. Hauch, S. D. Ebbesen, S. H. Jensen, M. Mogensen, J. Mater. Chem., 18 (2008), 2331-2340.

7. J. E. O'Brien, C. M. Stoots, J. S. Herring, J. J. Hartvigsen, Nucl. Technol., 158 (2007), 118-131.

8. S. H. Jensen, C. Graves, M. Mogensen, C. Wendel, R. Braun, G. Hughes, Z. Gao, S. A. Barnett, Energ Environ. Sci., 8 (2015), 2471-2479.

9. S. H. Chan, K. A. Khor, Z. T. Xia, J. Power Sources, 93 (2001), 130-140.

10. Y. Jiang, A. V. Virkar, J. Electrochem. Soc., 150 (2003), A942-A951.

11. R. E. Williford, L. A. Chick, G. D. Maupin, S. P. Simner, J. W. Stevenson, J. Electrochem. Soc., 150 (2003), A1067-A1072.

12. S.-L. Zhang, H. Wang, T. Yang, M. Y. Lu, C.-X. Li, C.-J. Li, S. A. Barnett, J. Mater. Chem. A, 8 (2020), 25867-25879.

13. T. Tsai, S. A. Barnett, Solid State Ionics, 98 (1997), 191-196.

14. J. S. Cronin, Y. C. K. Chen-Wiegart, J. Wang, S. A. Barnett, J. Power Sources, 233 (2013), 174-179.

15. H. Wang, Z. Gao, S. A. Barnett, J. Electrochem. Soc., 163 (2016), F196-F201.

16. K. J. Yoon, W. H. Huang, G. S. Ye, S. Gopalan, U. B. Pal, D. A. Seccombe, J.

Electrochem. Soc., 154 (2007), B389-B395.

17. K. J. Yoon, P. Zink, S. Gopalan, U. B. Pal, J. Power Sources, 172 (2007), 39-49.

18. D. Ding, X. Li, S. Y. Lai, K. Gerdes, M. Liu, Energy Environ. Sci., 7 (2014), 552-575.

19. D. Ding, M. Gong, C. Xu, N. Baxter, Y. Li, J. Zondlo, K. Gerdes, X. Liu, J. Power Sources, 196 (2011), 2551-2557.

20. S.-L. Zhang, H. Wang, M. Y. Lu, C.-X. Li, C.-J. Li, S. A. Barnett, J. Power Sources, 426 (2019), 233-241.

21. S.-L. Zhang, H. Wang, M. Y. Lu, A.-P. Zhang, L. V. Mogni, Q. Liu, C.-X. Li, C.-J. Li and S. A. Barnett, Energ Environ Sci., 11 (2018), 1870-1879.

22. S.-L. Zhang, D. Cox, H. Yang, B.-K. Park, C.-X. Li, C.-J. Li, S. A. Barnett, J Mater. Chem. A, 7 (2019), 21447-21458.

23. J. Kim, J. Kim, K. J. Yoon, J. W. Son, J. H. Lee, J. H. Lee, H. W. Lee, H. I. Ji, J. Alloy. Compd., 846 (2020), 156318.

24. J. Railsback, S. H. Choi, S. A. Barnett, Solid State Ionics, 335 (2019), 74-81.

25. M. Z. Khan, R. H. Song, M. T. Mehran, S. B. Lee, T. H. Lim, Ceram. Int., 2020, DOI: 10.1016/j.ceramint.2020.11.002.

26. Z. Gao, V. Y. Zenou, D. Kennouche, L. Marks, S. A. Barnett, J. Mater. Chem. A, 3 (2015), 9955-9964.

27. X. J. Chen, Q. L. Liu, S. H. Chan, N. P. Brandon, K. A. Khor, Electrochem. Commu., 9 (2007), 767-772.

28. M. E. Chelmehsara, J. Mahmoudimehr, Int. J. Hydrogen Energy, 43 (2018), 15521-15530.

29. A. Flura, C. Nicollet, S. Fourcade, V. Vibhu, A. Rougier, J. M. Bassat, J. C. Grenier, Electrochim. Acta, 174 (2015), 1030-1040.

30. F. W. Poulsen, Solid State Ionics, 129 (2000), 145-162.

31. B.-K. Park, R. Scipioni, Q. Zhang, D. Cox, P. W. Voorhees, S. A. Barnett, J Mater Chem A, 8 (2020), 11687-11694.

32. Q. Liu, Q. Zhang, P. W. Voorhees, S. A. Barnett, Journal of Phys. Energy, 2 (2019), 014006.

33. M. Chen, Y. L. Liu, J. J. Bentzen, W. Zhang, X. Sun, A. Hauch, Y. Tao, J. R. Bowen and P. V. Hendriksen, J. Electrochem. Soc., 160 (2013), F883-F891.

34. M. Kusnezoff, N. Trofimenko, M. Muller and A. Michaelis, Materials (Basel), 9 (2016), 906.

Fig. 1

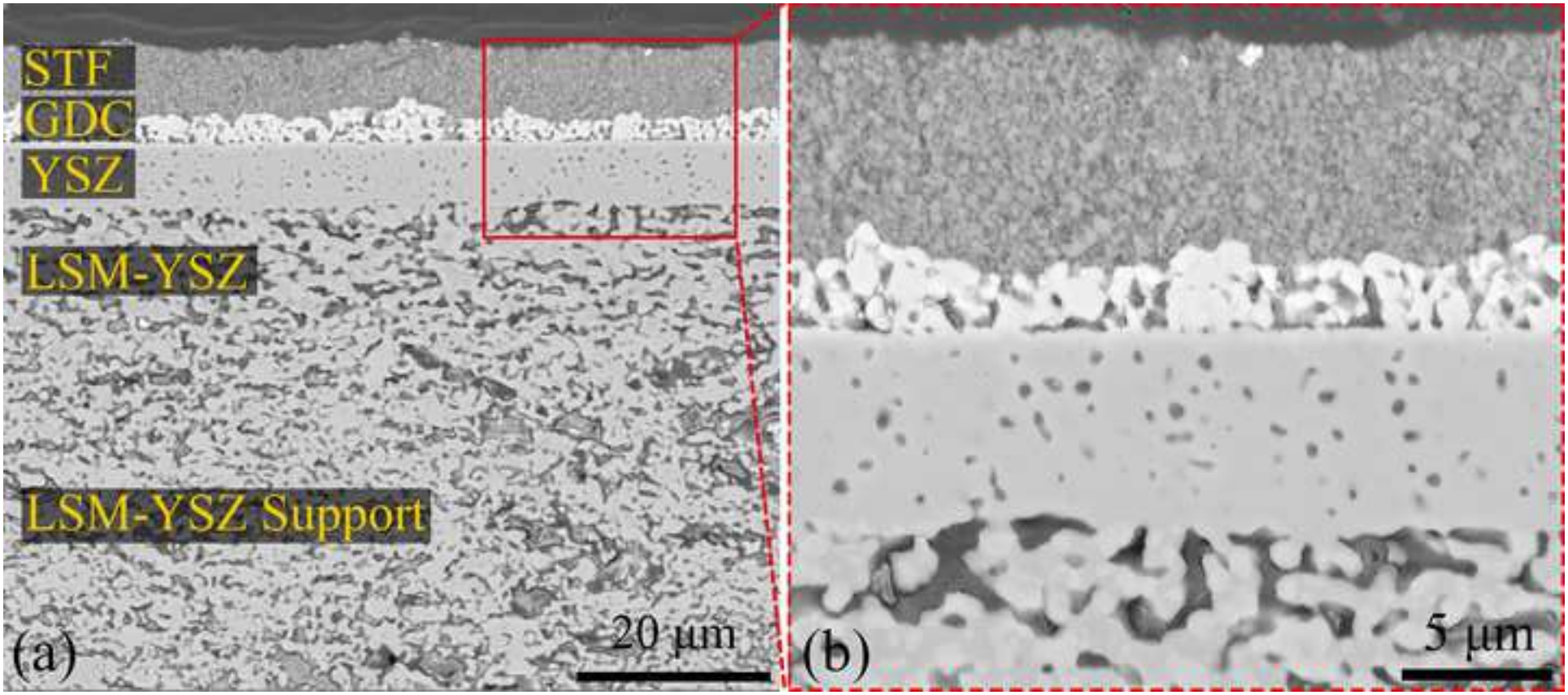

Fig. 2

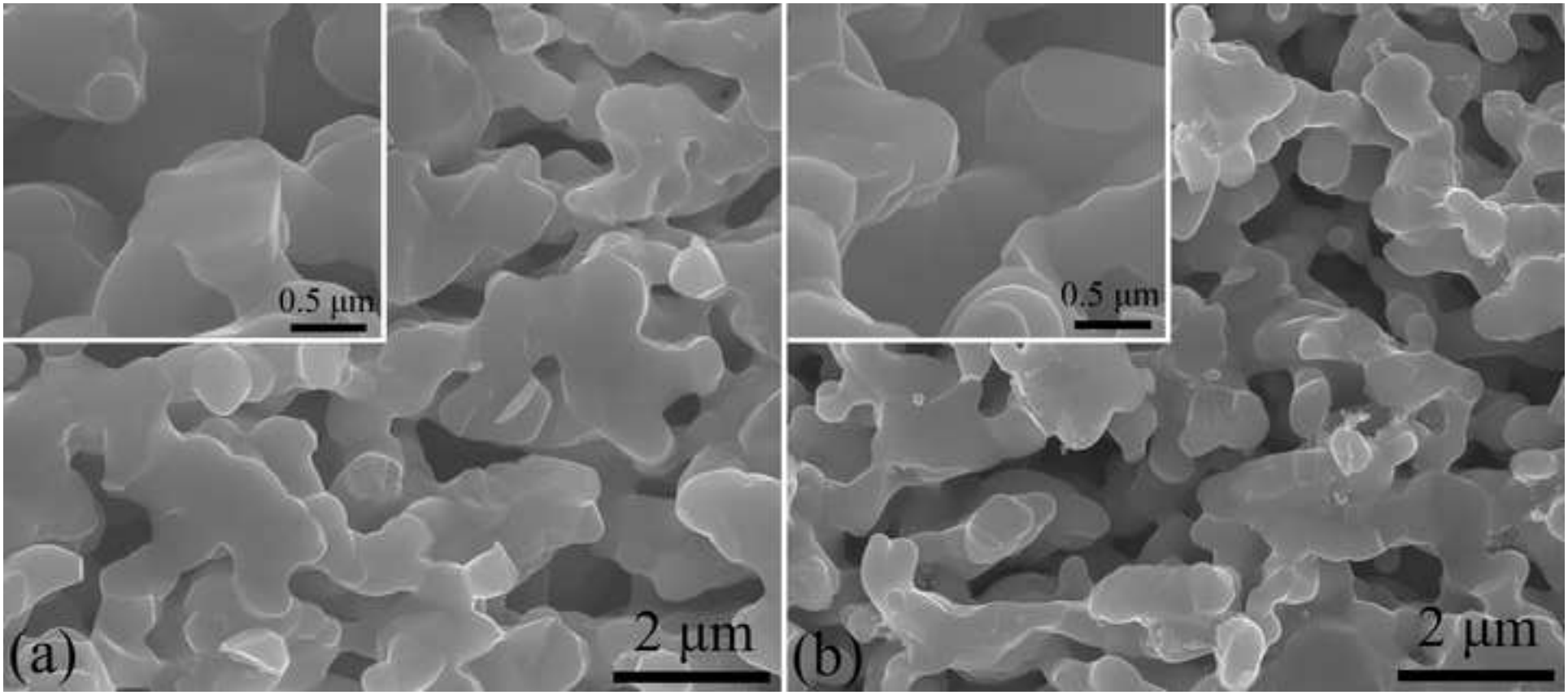

Fig. 3

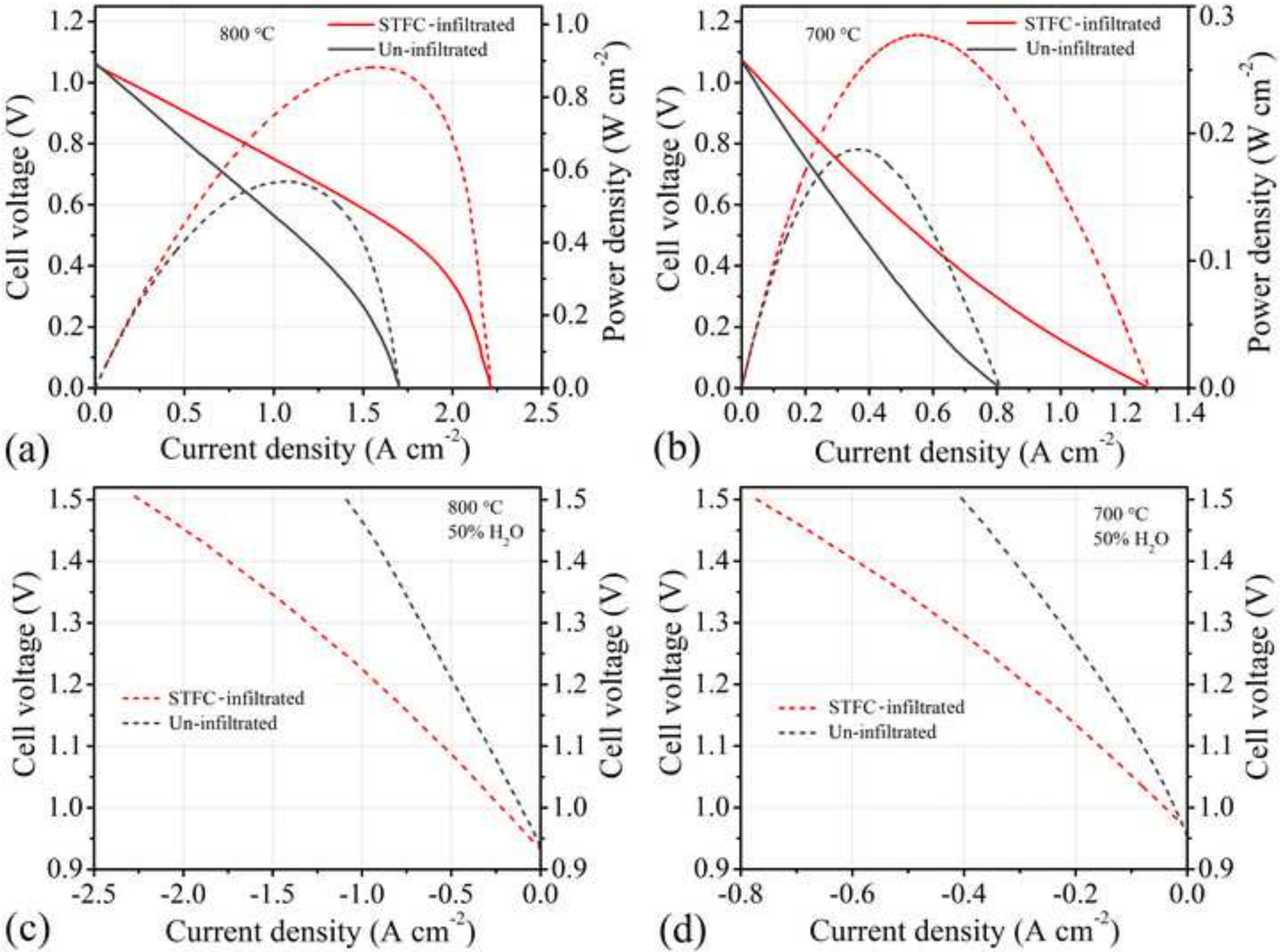

Fig. 4

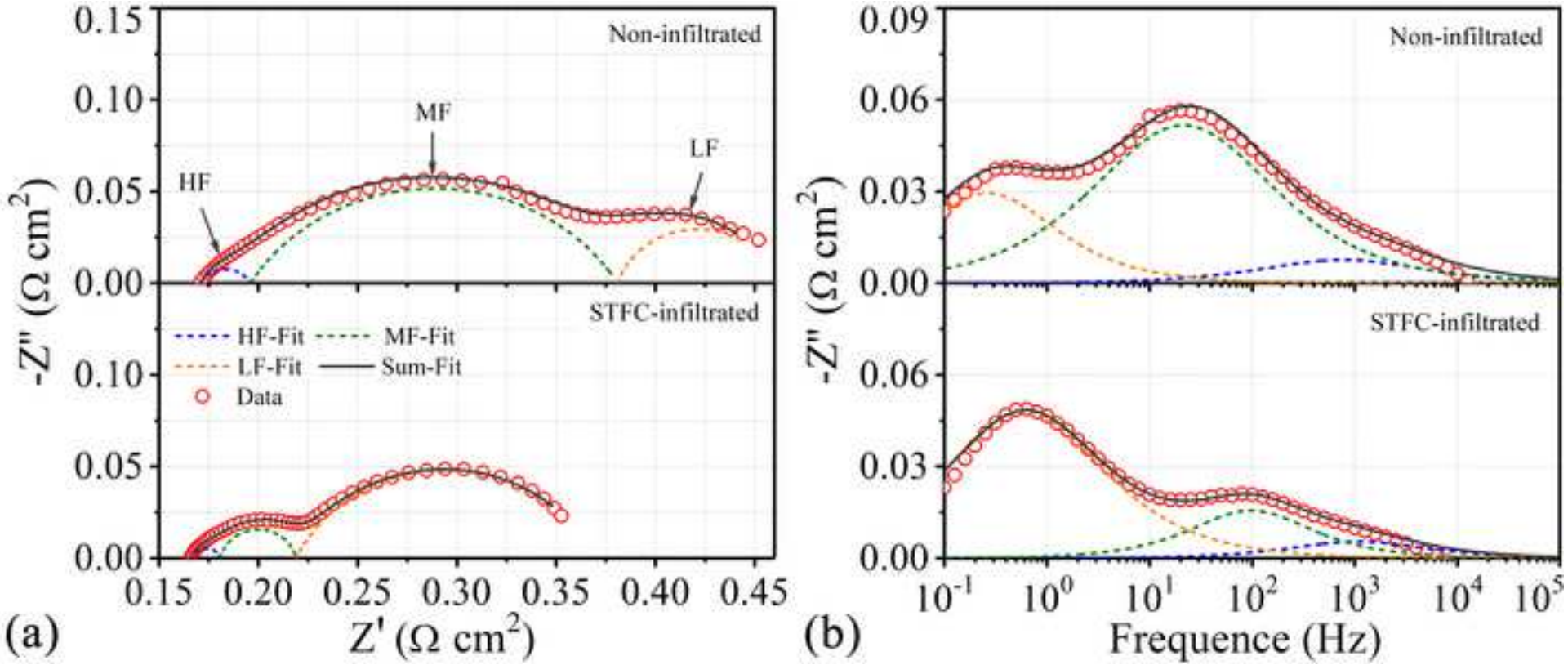

Fig. 5

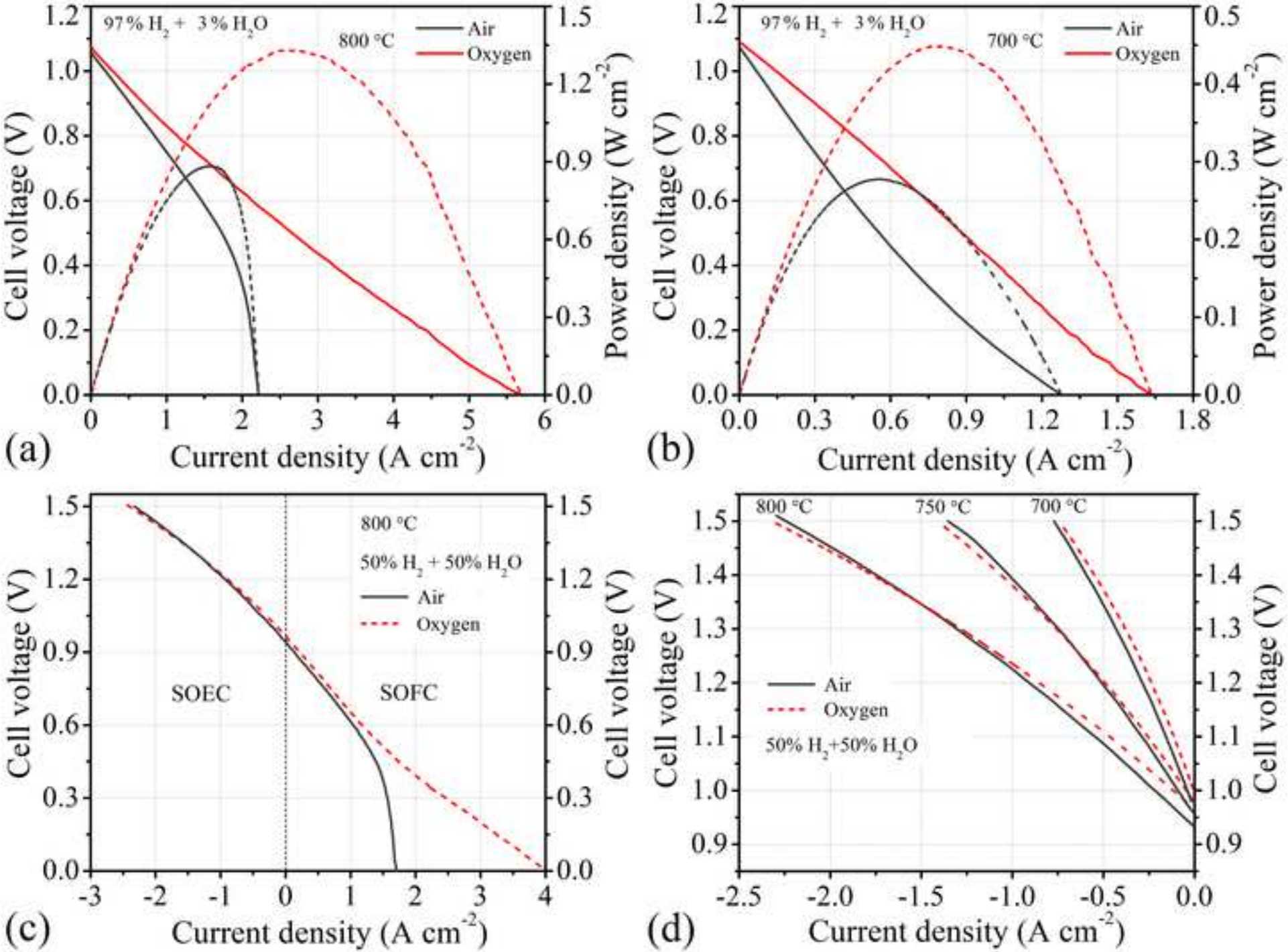

Fig. 6

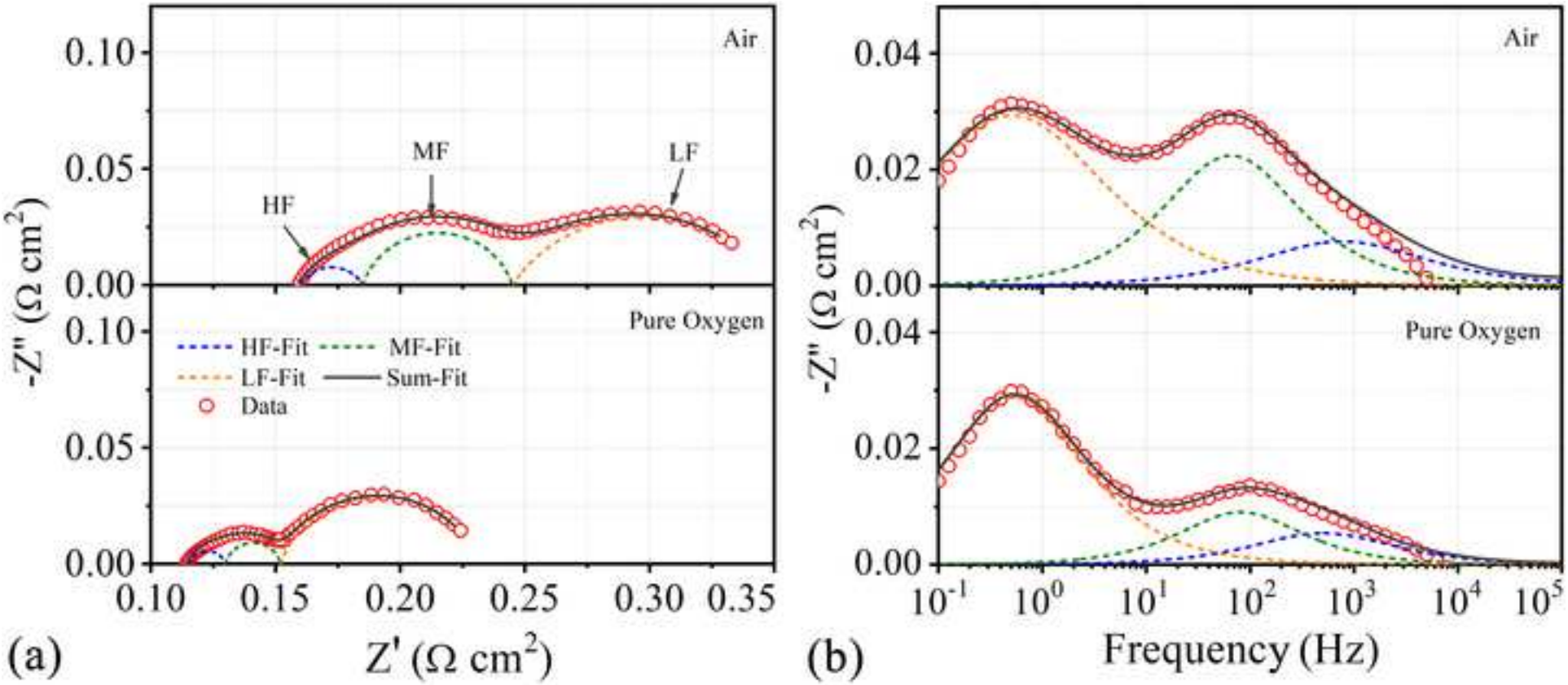

Fig. 1 Polished cross sectional SEM image of the cell (a) and a higher-magnification image of the cell's active region (b).

Fig. 2 Fracture cross-sectional SEM images of the un-infiltrated (a) and STFC-infiltrated (b) LSM-YSZ functional layer.

Fig. 3. Fuel cell voltage and power density versus current density for un-infiltrated and STFC-infiltrated cells measured in air and 97% H_2 - 3% H_2O at 800 °C (a) and 700 °C (b). Electrolysis voltage versus current density for un-infiltrated and STFC-infiltrated cells measured in air and 50% H_2 - 50% H_2O at 800 °C (c) and 700 °C (d).

Fig. 4 Nyquist (a) and Bode plots (b) of EIS data measured at 800 °C in 97% H_2 - 3% H_2O and air for cells with un-infiltrated and STFC-infiltrated LSM-YSZ electrodes.

Fig. 5. Voltage and power density versus current density for STFC-infiltrated cells comparing air and oxygen operation: in fuel cell mode with 97% H_2 - 3% H_2O at 800 °C (a) and 700 °C (b); in electrolysis and fuel cell modes with 50% H_2 - 50% H_2O at 800 °C (c); in electrolysis mode with 50% H_2 - 50% H_2O at 700, 750, and 800 °C.

Fig. 6 Nyquist (a) and Bode plots (b) of EIS data from STFC-infiltrated cells measured at 800 °C in 97% H_2 - 3% H_2O, with air or oxygen at the oxygen-electrode.